HHS Public Access

Author manuscript

J Neurooncol. Author manuscript; available in PMC 2018 May 01.

Published in final edited form as:

J Neurooncol. 2017 May ; 133(1): 9–16. doi:10.1007/s11060-017-2410-3.

Can anti-Vascular Endothelial Growth Factor Antibody Reverse Radiation Necrosis? A Preclinical Investigation

Chong Duan[1], **Carlos J Perez-Torres**[2], **Liya Yuan**[3], **John A Engelbach**[4], **Scott C Beeman**[2], **Christina I Tsien**[4], **Keith M Rich**[3,4], **Robert E Schmidt**[5], **Joseph JH Ackerman**[1,2,6,7], and **Joel R Garbow**[2,7,*]

[1]Department of Chemistry, Washington University, Saint Louis, Missouri, United States

[2]Department of Radiology, Washington University, Saint Louis, Missouri, United States

[3]Department of Neurosurgery, Washington University, Saint Louis, Missouri, United States

[4]Department of Radiation Oncology, Washington University, Saint Louis, Missouri, United States

[5]Department of Pathology and Immunology, Washington University, Saint Louis, Missouri, United States

[6]Department of Medicine, Washington University, Saint Louis, Missouri, United States

[7]Alvin J Siteman Cancer Center, Washington University, Saint Louis, Missouri, United States

Abstract

Anti-vascular endothelial growth factor (anti-VEGF) antibodies are a promising new treatment for late time-to-onset radiation-induced necrosis (RN). We sought to evaluate and validate the response to anti-VEGF antibody in a mouse model of RN. Mice were irradiated with the Leksell Gamma Knife Perfexion^{TM} and then treated with anti-VEGF antibody, beginning at post-irradiation (PIR) week 8. RN progression was monitored *via* anatomic and diffusion MRI from weeks 4 to 12 PIR. Standard histology, using haematoxylin and eosin (H&E), and immunohistochemistry staining were used to validate the response to treatment. After treatment, both post-contrast T1-weighted and T2-weighted image-derived lesion volumes decreased (P<0.001), while the lesion volumes for the control group increased. The abnormally high apparent diffusion coefficient (ADC) for RN also returned to the ADC range for normal brain following treatment (P<0.001). However, typical RN pathology was still present histologically. Large areas of focal calcification were observed in ~50% of treated mouse brains. Additionally, VEGF and hypoxia-inducible factor 1-alpha (HIF-1α) were continually upregulated in both the anti-VEGF and control groups. Despite improvements observed radiographically following anti-VEGF treatment, lesions were not completely resolved histologically. The subsequent calcification

*Corresponding Author: Joel R Garbow, Ph.D., Biomedical MR Laboratory, Campus Box 8227, Washington University School of Medicine, Room 2313, 4525 Scott Ave, St Louis, MO 63110, USA, Phone : +1 314 362 9949, Fax : +1 314 362 0526, garbow@wustl.edu.

Conflict of interest: The authors declare that they have no conflict of interest.

Ethical approval: All applicable international, national, and/or institutional guidelines for the care and use of animals were followed.

Ethical approval: This article does not contain any studies with human participants performed by any of the authors.

and the continued upregulation of VEGF and HIF-1α merit further preclinical/clinical investigation.

Keywords

Radiation Necrosis; VEGF; bevacizumab; Diffusion; HIF-1α; Calcification

Introduction

Radiation-induced necrosis (RN), with clinical symptoms mimicking those of tumor recurrence, is a late time-to-onset, devastating complication following radiotherapy to the central nervous system [1–3]. Traditionally, RN has been treated with corticosteroid [4] to control edema and lessen inflammatory responses. However, the long-term use of corticosteroid is associated with chronic side effects, including hyperglycemia and immunosuppression. Anticoagulants agents (e.g., heparin and warfarin) [5] and hyperbaric oxygen therapy [6] have also been used in an attempt to heal microvasculature impairments and improve regional cerebral blood supply, but results have been inconsistent and disappointing [7]. Recently, RN in the brain has been treated clinically using bevacizumab (Avastin©, Genentech, San Francisco, CA), an anti-vascular endothelial growth factor (VEGF) antibody hypothesized to restore blood brain barrier (BBB) function and, thereby, to repair vascular leakage [7–9].

While bevacizumab improves neurological symptoms and reduces the volume of RN-associated vascular leakage and resultant edema detected radiographically, the treatment brings with it potentially serious complications [10–12]. For instance, bevacizumab treatment increases the risk of hemorrhage and retards wound healing by impairing neovascularization, which are critical concerns for neurosurgeons [12, 13]. Also, Levin et al [14] reported clinically significant toxicity, including deep-vein thrombosis, and superior-sagittal-sinus thrombosis, in 6 of 11 bevacizumab-treated patients. Deterioration/rebound phenomena after an initial positive response with/without continued therapy have also been documented [15–17]. A comprehensive study of the treatment effect, validated with gold-standard histology, is warranted. Preclinical models present a unique opportunity to study the effects of anti-VEGF antibody treatment on pure RN, independent of the potentially obfuscating complications of other pathologies, including recurrent tumors.

We have previously investigated the mitigative effect of anti-VEGF antibody on RN [18] and the specificity of this effect [19], in which the irradiated mice were treated starting from the *initial* appearance of RN on anatomic MR (approximately 4 weeks post irradiation). Motivated by ongoing clinical trials using bevacizumab to treat *frank* RN, in the present study we evaluate the anti-VEGF antibody treatment with a preclinical protocol mimicking the more clinically relevant situation. Specifically, anti-VEGF antibody treatment is not administered until a moderate-size region of focal RN developed at the irradiation site. Both anatomic and diffusion-weighted MRI were employed to monitor changes in the lesions as functions of both treatment and time post irradiation. We also evaluated the treatment responses using standard haematoxylin and eosin (H&E) and immunohistochemical (IHC)

stains, an evaluation that is, generally, impractical in humans due to the lack of appropriate tissue samples.

Material and methods

Animal Model

All experiments were approved by the Washington University Animal Studies Committee and were performed on six-to-eight week old female BALB/c mice (Harlan/Envigo, Indianapolis, IN, USA). A single-fraction, 50-Gy dose of radiation (50% isodose) from the Leksell Gamma Knife™ Perfexion™ (Elekta, Stockholm, Sweden) was focused on the cortex of the left hemisphere (n = 24). As has been shown previously [18–20], this large, single-fraction dose of radiation reproducibly and robustly generates, in all irradiated mice, radiation necrosis whose histology recapitulates all of the features of clinical RN. At this dose, moderate focal RN can be observed at approximately 8 weeks post irradiation (PIR) on both anatomic MRI and histology [20]. B20-4.1.1, a murine antibody that recognizes VEGF, and GP120:9239, a murine antibody of the same isotype that targets the HIV capsid protein, were obtained from Genentech (South San Francisco, CA, USA). At week 8 PIR, mice were randomly divided into two groups: (i) an anti-VEGF group, treated with B20-4.1.1 and (ii) an isotype-control group, treated with GP120:9239. Each antibody was administrated intraperitoneally at 10 mg/kg twice weekly until week 12 PIR. To minimize the acute effect of blocking VEGF activity on permeability and therefore contrast-agent extravasation, all MRI scans were performed two days following a treatment.

Magnetic Resonance Imaging

Images were acquired with a 4.7-T small-animal Agilent/Varian (Santa, Clara, CA) DirectDrive™ scanner using an actively decoupled transmit (volume, 9-cm inner diameter) and receive (surface, 1.5-cm outer diameter) coil pair. Mice were placed on a warm water pad and anesthetized with isoflurane/O_2 (1% isoflurane) throughout the experiment. Before loading into the magnet, mice were given an intraperitoneal injection of 0.25 mL MultiHance (gadobenate dimeglumine; Bracco Diagnostics, Princeton, NJ) contrast agent, diluted 1:5 in sterile saline. Post-contrast T1-weighted (T1W, TR/TE = 650/16 ms) and T2-weighted (T2W, TR/TE = 1500/50 ms), spin-echo transaxial images were acquired every other week from week 4 PIR to week 12 PIR. A total of 21 contiguous slices with 0.5 mm thickness and 15 × 15 mm^2 field of view (128 × 128 matrix) were collected. Diffusion-weighted images (DWI) were acquired at week 8 PIR (pre-treatment) and week 12 PIR (post-treatment) employing a diffusion weighted spin-echo sequence. Three separate diffusion datasets with the diffusion-encoding gradient applied along three orthogonal directions (b = 1000 s/mm^2), and a reference dataset, without diffusion gradient (b = 0), were acquired for each animal with the same field of view as the post-contrast T1W and T2W images.

Data analysis

RN volumes were derived from both post-contrast T1W and T2W images, as previously described [21], using custom-written Matlab software (The Mathworks, Natick, MA). Briefly, each mouse brain was divided along the midline into left (irradiated) and right (non-

irradiated) hemispheres. The intensity of each pixel in the left hemisphere was normalized by the average intensity of 25 pixels (5×5 square) surrounding its mirror-image pixel in the right hemisphere. The lesion volumes were then determined *via* a threshold segmentation algorithm, in which areas of the left hemisphere brighter than the 95th percentile of the right hemisphere (i.e., an intensity threshold of roughly 1.4x that of the mean normalized pixel intensity) were defined as lesions. In addition, areas darker than the 95th percentile of the right hemisphere (i.e., a threshold of roughly 0.6) were also classified as lesions to account for hypo-intense regions caused by hemorrhage. For DWI experiments, apparent diffusion coefficient (ADC) maps were calculated as the average of the diffusion coefficients calculated from the three separate diffusion datasets and the reference dataset. For both groups, RN lesion ROIs were defined on the post-contrast T1W images at week 8 PIR and overlaid onto the ADC maps. Each week-12 PIR image was co-registered (affine transformation to allow for possible scaling changes caused by brain swelling) to its corresponding week-8 PIR image. The same ROI drawn in week 8 was then overlaid onto the corresponding week-12 image. The median value for the ADC across the ROI was calculated for comparison between pre- and post-treatment datasets. Statistical analyses for both RN volumes and median ADCs were performed using a paired-sample, two-sided *t*-test.

Histology and IHC

All mice were sacrificed immediately after the last imaging time point (week 12 PIR) and intracardially perfused with 1% phosphate-buffered saline (PBS, PH = 7.4) and 10% formalin. Mice heads were dissected and immersed in formalin for 24 hours. Brains were removed from the skulls and a 3-mm thick transaxial block, centered at the irradiation site (~3 mm behind the bregma), was obtained for each brain. The blocks were then processed through graded alcohols and embedded in paraffin. All paraffin- fixed blocks were sectioned from their centers at a thickness of five microns. Tissue sections were stained with haematoxylin and eosin (H&E) according to standard protocols. Immunohistochemical staining (IHC) for both VEGF and HIF-1α was performed following the manufacturers' protocols. Antigen retrieval was performed with citrate buffer (pH = 6.8) at 70°C overnight following one-hour non-specific blocking. Rabbit anti-VEGF (orb11553, Biorbyt, Cambridge, UK) at 1:500 and Rabbit anti-HIF-1α (NB100-479, Novus Biotechnology, Littleton, CO, USA) at 1:300 were used as primary antibodies at 4°C overnight, and diaminobenzidine (DAB) staining was performed using the Histostain Plus Broad System kit (Invitrogen, Frederick, MD, USA). All sections were incubated with a broad-spectrum secondary antibody for one hour and with horseradish peroxidase streptavidin (HRP-streptavidin) for 30 minutes. Staining was visualized with a DAB precipitation reaction. Histological slides were examined with the Hamamatsu NanoZoomer whole-slide imaging system (Hamamatsu, Hamamatsu City, Japan).

Results

RN volume is decreased after anti-VEGF antibody treatment

Both the anti-VEGF antibody-treated and isotype-control antibody-treated mice were imaged biweekly from weeks 4 to 12 PIR. Figure 1 shows representative post-contrast T1W

and T2W images for both groups at week 8 (pre-treatment) and week 12 (post-treatment) PIR. RN lesions appear bright in these images. Note that anti-VEGF treatment reduced swelling (smaller brain sizes), while the brains continued to swell for the isotype-control group. Post-contrast, T1W-derived lesion volumes decreased after anti-VEGF treatment from 51.3 ± 19.0 to 24.6 ± 14.8 mm^3 ($P<0.001$), while the lesion volumes of the isotype-control antibody treated group increased from 55.4 ± 27.0 to 101.9 ± 42.9 mm^3 ($P<0.001$). Similarly, T2W-derived lesion volumes decreased after anti-VEGF treatment from 45.9 ± 15.5 to 21.7 ± 13.5 mm^3 ($P<0.001$), while the lesion volumes of the isotype-control group increased from 40.5 ± 15.8 to 84.9 ± 28.4 mm^3 ($P<0.001$). Note that T2W-derived lesion volumes are slightly smaller than post-contrast T1W-derived volumes, consistent with results reported previously [19].

ADC is reversed after the treatment

Diffusion-weighted images were collected at weeks 8 and 12 PIR. Figure 2 (left) shows ADC maps for representative members of both groups. Compared to the contralateral side, the RN lesion demonstrates abnormally high ADC, as described previously [21]. Boxplots in the right panel of Fig. 2 show that median ADCs across the lesion decreased from 0.95 ± 0.07 to 0.73 ± 0.04 $\mu m^2/ms$ ($P<0.001$) for the anti-VEGF treated mice, while the median ADCs for the isotype-control group remain unchanged. For reference, the ADC for normal brain (0.68 ± 0.02 $\mu m^2/ms$) is computed from ROIs drawn in the contralateral hemisphere. For this healthy brain-tissue reference ADC measurement, only contralateral regions of anti-VEGF-treated animals are included, to avoid possible contamination from contralateral lesions observed previously in a small number of non-treated mice at late time points [22].

RN is not completely resolved histologically after treatment

To validate the treatment responses observed by MRI, standard H&E staining of brain tissue was performed for each mouse. Consistent with the clinical scenario, H&E staining of lesions in the isotype-control group display all of the classic RN-related pathologies, including telangiectasia, hyalinization, fibrinoid vascular necrosis, hemorrhage, and tissue loss (Fig. 3, left panel). These histologic features, though reduced in extent, are also observed in the brains of the anti-VEGF antibody treated mice (Fig. 3, middle panel). In addition, large areas of focal mineralization (dystrophic calcification) were observed in roughly half of the anti-VEGF treated mice (Fig. 3, right panel), while none of the isotype-control antibody treated brains showed any mineral deposits.

VEGF and HIF-1α remain upregulated after treatment

Immunohistochemistry was performed to evaluate the expression levels of VEGF and HIF-1α, a well-known transactivator of VEGF, following anti-VEGF antibody treatment, for all mice in both groups. As a negative control, the same IHC staining protocols were also performed on non-irradiated, age-matched female mice (Fig. 4, left panel). As expected, for the necrotic tissue, Fig. 4 (middle panel) shows that both VEGF and HIF-1α were upregulated for the isotype-control group, especially along the walls of the dilated blood vessels. However, despite the anti-VEGF antibody treatment and less RN-associated pathologies shown in Fig. 3, both VEGF and HIF-1α remained upregulated for the anti-VEGF group (Fig. 4, right panel).

Discussion

Cerebral radiation necrosis can be a serious consequence following radiotherapy. Traditional treatments of RN, including corticosteroids and hyperbaric oxygen, are associated with significant toxicity and limited efficacy [23]. Recently, multiple groups have investigated the treatment effect of anti-VEGF antibody (i.e., bevacizumab), which blocks VEGF from reaching its capillary target and is, thus, hypothesized to reduce vascular leakage and associated brain edema, on radiographic volumes of RN clinically [7–10]. The work presented herein is distinct from prior clinical studies in that the Gamma Knife mouse RN model is a single hemisphere radiation injury model, which allows (i) direct comparisons with the non-irradiated hemisphere and (ii) histological validations that are impractical for clinical cases. The model is also independent of potential complications arising from other pathologies, including recurrent tumor.

Consistent with prior clinical investigations [7–10], anti-VEGF treated mice show remarkable decreases of RN lesion volume, detected radiographically on both post-contrast T1W and T2W images (Fig. 1). This finding is correlated with the smaller lesion volume, and less vasogenic edema, on H&E-stained brain tissue in treated group *vs.* untreated group. The swelling of the irradiated brains is also reduced by the treatment. In addition to anatomic images, diffusion MRI, whose metrics reflect the barriers and restrictions to the incoherent displacement of water molecules, was also investigated. We showed that the abnormally high ADC associated with RN was reduced to more normal levels (Fig. 2), an effect that is likely due to decreased vasogenic edema and brain swelling.

Building upon the results of our previous work, in which anti-VEGF treatment was initiated at the *initial* radiologic appearance of RN, the current study addresses the more clinically relevant problem in which treatment is not started until after the development of regions of *frank* RN. While in our earlier study the treated mice displayed almost no visible tissue damage by histology (H&E), typical RN histologic pathologies and large areas of focal mineral deposits are present after the anti-VEGF treatment in the current study. Jeyaretna et al [15] reported a worsening clinical scenario after bevacizumab treatment of histologic diagnosis-confirmed RN. In a follow-up, image-guided surgical biopsy, large areas of focal dystrophic calcification were observed in the lesion. It was hypothesized the prolonged anti-VEGF treatment resulted in overpruning of at-risk blood vessels, leading to vascular deficiency, which eventually exacerbated the lesion. The connection between vascular deficiency and the observed dystrophic calcification is unclear and requires further study.

The pathophysiology of RN remains incompletely understood. The current consensus views RN as a continuous, complex process from endothelial-cell dysfunction to tissue hypoxia and necrosis, with concomitant upregulation of both HIF-1α and VEGF [24, 25]. As expected, we found that both VEGF and the HIF-1α are upregulated for the isotype-control group, consistent with limited clinical biopsy results. Both VEGF and HIF- 1α remain upregulated in the treatment group, which may contribute to the risk of recurrence of RN lesions. This finding is consistent with the mechanism of action of the anti-VEGF antibody, which binds and, thus, blocks the function of VEGF and its bioactive fragments, but does not reduce/eliminate VEGF expression. In this regard, directly targeting of its upstream

transactivator, HIF-1a, may represent a feasible approach for reducing the expression of VEGF. On the other hand, VEGF is a homodimeric glycoprotein that acts *via* endothelial-specific receptor tyrosine kinases (e.g., VEGFR2). Thus, blocking these receptors may also help to reduce RN recurrence despite the continued upregulation of VEGF itself.

The observed reduction in radiographically detected lesion volume in mice is consistent with the improvement in clinical symptoms seen in RN patients following treatment with bevacizumab [14]. However, neither post-contrast T1W nor T2W imaging contrasts provide direct readouts of RN pathologies. Post-contrast T1W is sensitive to vascular permeability, while T2W is sensitive to the brain edema resulted from the vascular leakage. It is not surprising that the anti-VEGF antibody, which mediates the BBB dysfunction, reduces the lesion volumes derived from these images. However, further tissue changes/damage within the necrotic area, including neuronal necrosis and vascular necrosis, may be permanent and irreversible. Such pathology could be “invisible” on these images after anti-VEGF treatment.

One major limitation/side effect of anti-VEGF antibody treatment is that it impairs neovascularization and retards wound healing. Consequently, the timing of surgery in neurosurgical patients treated with anti-VEGF therapy must be carefully considered [12]. Additionally, although this study demonstrated that anti-VEGF antibody treatment can reduce radiographically observed RN lesion volume, it did not address important questions about optimal dosing schemes and treatment periods. The use of a lower antibody dose and shorter treatment periods could potentially minimize side effects and improve patient care.

In summary, we found anti-VEGF antibody decreased RN lesion volumes on post-contrast T1W and T2W in a Gamma Knife mouse RN model. In addition, the abnormally high RN ADCs were reduced to values typical of normal brain. However, the lesions were not completely resolved histologically. The subsequent calcification and the continued upregulation of VEGF and HIF-1α merit further clinical and pre-clinical investigation. More effective treatments, possibly aimed at targets either upstream (e.g., HIF-1α) or downstream (e.g., VEGFR2) of VEGF, and monitoring of the neurological behavior of irradiated animals, pre- and post-treatment, will be the subject of future studies.

Acknowledgments

This project was supported by NIH Grant R01 CA155365 (J.R.G), funding from the Alvin J. Siteman Cancer Center (P30 CA091842), the Barnes-Jewish Hospital Foundation Cancer Frontier Fund, and Elekta Instruments AB (Stockholm, Sweden). We acknowledge Genentech for donation of the antibodies B20-4.1.1 and GP120:9239 and thank Mr. Jeremy Cates for his help with the irradiation of the mice.

Funding: This study was funded by NIH grant R01 CA155365 and P30 CA091842, the Barnes-Jewish Hospital Foundation Cancer Frontier Fund, and Elekta Instruments AB (Stockholm, Sweden).

References

1. Giglio P, Gilbert MR. Cerebral radiation necrosis. The neurologist. 2003; 9:180–188. [PubMed: 12864928]
2. Kumar AJ, Leeds NE, Fuller GN, et al. Malignant Gliomas: MR Imaging Spectrum of Radiation Therapy-and Chemotherapy-induced Necrosis of the Brain after Treatment 1. Radiology. 2000; 217:377–84. [PubMed: 11058631]

3. Rahmathulla G, Marko NF, Weil RJ. Cerebral radiation necrosis: a review of the pathobiology, diagnosis and management considerations. J Clin Neurosci. 2013; 20:485–502. [PubMed: 23416129]
4. Shaw PJ, Bates D. Conservative treatment of delayed cerebral radiation necrosis. J Neurol Neurosurg Psychiatry. 1984; 47:1338–1341. [PubMed: 6512555]
5. Glantz MJ, Burger PC, Friedman AH, et al. Treatment of radiation-induced nervous system injury with heparin and warfarin. Neurology. 1994; 44:2020–2020. [PubMed: 7969953]
6. Bui Q-C, Lieber M, Withers HR, et al. The efficacy of hyperbaric oxygen therapy in the treatment of radiation-induced late side effects. Int J Radiat Oncol. 2004; 60:871–878. DOI: 10.1016/j.ijrobp.2004.04.019
7. Gonzalez J, Kumar AJ, Conrad CA, Levin VA. Effect of bevacizumab on radiation necrosis of the brain. Int J Radiat Oncol Biol Phys. 2007; 67:323–326. DOI: 10.1016/j.ijrobp.2006.10.010 [PubMed: 17236958]
8. Torcuator R, Zuniga R, Mohan YS, et al. Initial experience with bevacizumab treatment for biopsy confirmed cerebral radiation necrosis. J Neurooncol. 2009; 94:63–8. [PubMed: 19189055]
9. Bölke E, Nawatny J, Hoffmann TK, et al. Bevacizumab as a treatment option for radiation-induced cerebral necrosis. Strahlenther Onkol. 2011; 187:135–9. [PubMed: 21336713]
10. Lubelski D, Abdullah KG, Weil RJ, Marko NF. Bevacizumab for radiation necrosis following treatment of high grade glioma: a systematic review of the literature. J Neurooncol. 2013; 115:317–322. DOI: 10.1007/s11060-013-1233-0 [PubMed: 24005770]
11. Scappaticci FA, Fehrenbacher L, Cartwright T, et al. Surgical wound healing complications in metastatic colorectal cancer patients treated with bevacizumab. J Surg Oncol. 2005; 91:173–80. DOI: 10.1002/jso.20301 [PubMed: 16118771]
12. Abrams DA, Hanson JA, Brown JM, et al. Timing of surgery and bevacizumab therapy in neurosurgical patients with recurrent high grade glioma. J Clin Neurosci. 2015; 22:35–39. [PubMed: 25481268]
13. Clark AJ, Butowski NA, Chang SM, et al. Impact of bevacizumab chemotherapy on craniotomy wound healing: Clinical article. J Neurosurg. 2011; 114:1609–16. [PubMed: 21142749]
14. Levin VA, Bidaut L, Hou P, et al. Randomized Double-Blind Placebo-Controlled Trial of Bevacizumab Therapy for Radiation Necrosis of the Central Nervous System. Int J Radiat Oncol. 2011; 79:1487–95. DOI: 10.1016/j.ijrobp.2009.12.061
15. Jeyaretna DS, Curry WT, Batchelor TT, et al. Exacerbation of Cerebral Radiation Necrosis by Bevacizumab. J Clin Oncol. 2011; 29:e159–e162. DOI: 10.1200/JCO.2010.31.4815 [PubMed: 21149667]
16. Furuse M, Kawabata S, Kuroiwa T, Miyatake S-I. Repeated treatments with bevacizumab for recurrent radiation necrosis in patients with malignant brain tumors: a report of 2 cases. J Neurooncol. 2010; 102:471–475. DOI: 10.1007/s11060-010-0333-3 [PubMed: 20694573]
17. Wang Y, Pan L, Sheng X, et al. Reversal of cerebral radiation necrosis with bevacizumab treatment in 17 Chinese patients. Eur J Med Res. 2012; 17:25.doi: 10.1186/2047-783X-17-25 [PubMed: 22913802]
18. Jiang X, Engelbach JA, Yuan L, et al. Anti-VEGF Antibodies Mitigate the Development of Radiation Necrosis in Mouse Brain. Clin Cancer Res. 2014; 20:2695–2702. DOI: 10.1158/1078-0432.CCR-13-1941 [PubMed: 24647570]
19. Perez-Torres CJ, Yuan L, Schmidt RE, et al. Specificity of vascular endothelial growth factor treatment for radiation necrosis. Radiother Oncol. 2015; 117:382–385. DOI: 10.1016/j.radonc.2015.09.004 [PubMed: 26376163]
20. Jiang X, Yuan L, Engelbach JA, et al. A Gamma-Knife-Enabled Mouse Model of Cerebral Single-Hemisphere Delayed Radiation Necrosis. PLOS ONE. 2015; 10:e0139596.doi: 10.1371/journal.pone.0139596 [PubMed: 26440791]
21. Perez-Torres CJ, Engelbach JA, Cates J, et al. Toward Distinguishing Recurrent Tumor From Radiation Necrosis: DWI and MTC in a Gamma Knife Irradiated Mouse Glioma Model. Int J Radiat Oncol. 2014; 90:446–453. DOI: 10.1016/j.ijrobp.2014.06.015
22. Perez-Torres CJ, Yuan L, Schmidt RE, et al. Perilesional edema in radiation necrosis reflects axonal degeneration. Radiat Oncol Lond Engl. 2015; 10:33.doi: 10.1186/s13014-015-0335-6

23. Miyatake S-I, Nonoguchi N, Furuse M, et al. Pathophysiology, Diagnosis, and Treatment of Radiation Necrosis in the Brain. Neurol Med Chir (Tokyo). 2014; doi: 10.2176/nmc.ra.2014-0188

24. Wong CS, Van der Kogel AJ. Mechanisms of radiation injury to the central nervous system: implications for neuroprotection. Mol Interv. 2004; 4:273–284. DOI: 10.1124/mi.4.5.7 [PubMed: 15471910]

25. Yoritsune E, Furuse M, Kuwabara H, et al. Inflammation as well as angiogenesis may participate in the pathophysiology of brain radiation necrosis. J Radiat Res (Tokyo). 2014; 55:803–811. DOI: 10.1093/jrr/rru017 [PubMed: 24676944]

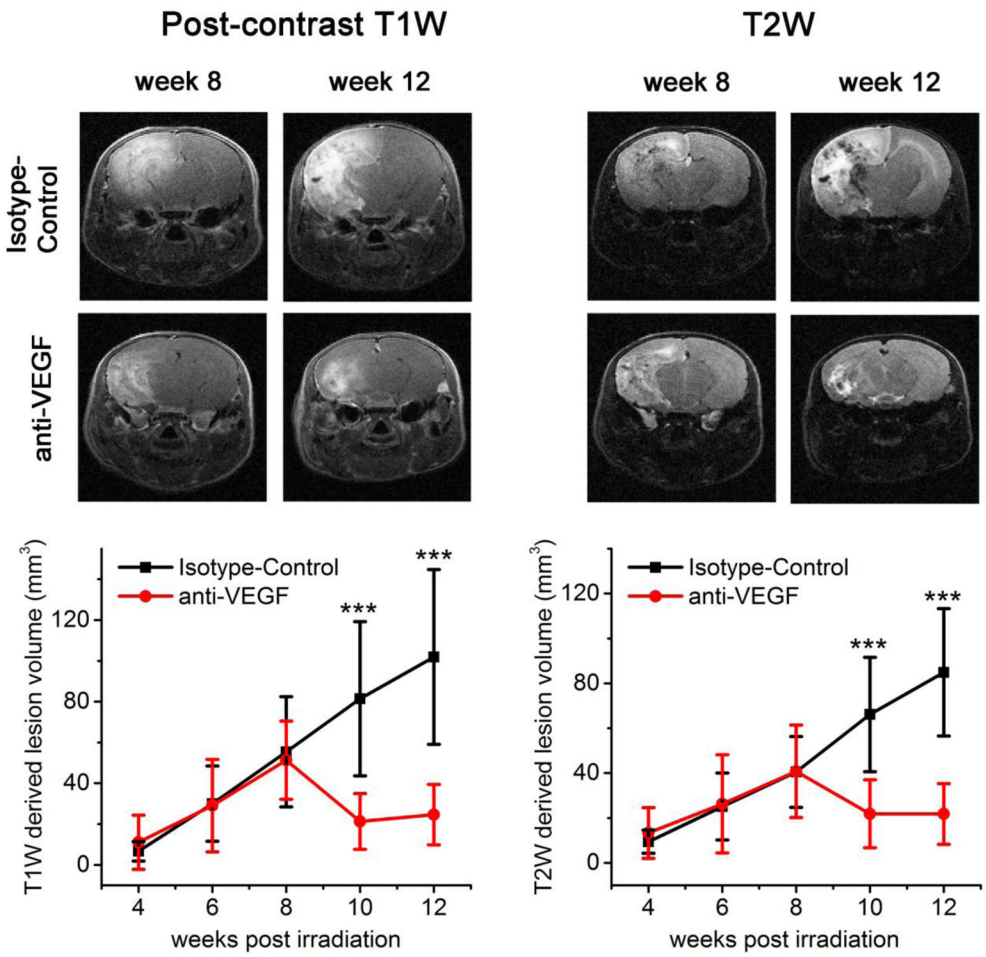

Fig. 1.

Anti-VEGF treatment response detected by anatomic MRI. The top panels show images at week 8 PIR (pre-treatment) and week 12 PIR (post-treatment) for one representative mouse in both isotype-control and anti-VEGF groups. The bottom panels are plots of MR-derived lesion volumes (mean ± SD, n = 12) versus time after irradiation for both groups (*black* isotype-control group; *gray* anti-VEGF group). "***"Indicate $P<0.001$ as calculated by a paired-sample *t* test

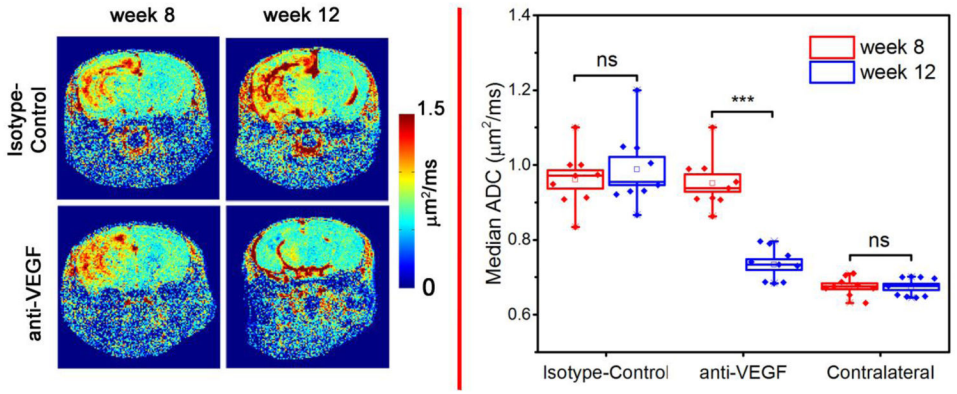

Fig. 2.

Anti-VEGF treatment response, detected by diffusion-weighted MRI. The left panels display representative ADC maps. *Boxplots* (n = 9), on the *right*, show median ADCs across the lesions. The contralateral group represents normal brain ADCs. "***" and "ns" indicate $P<0.001$ and no significance, respectively

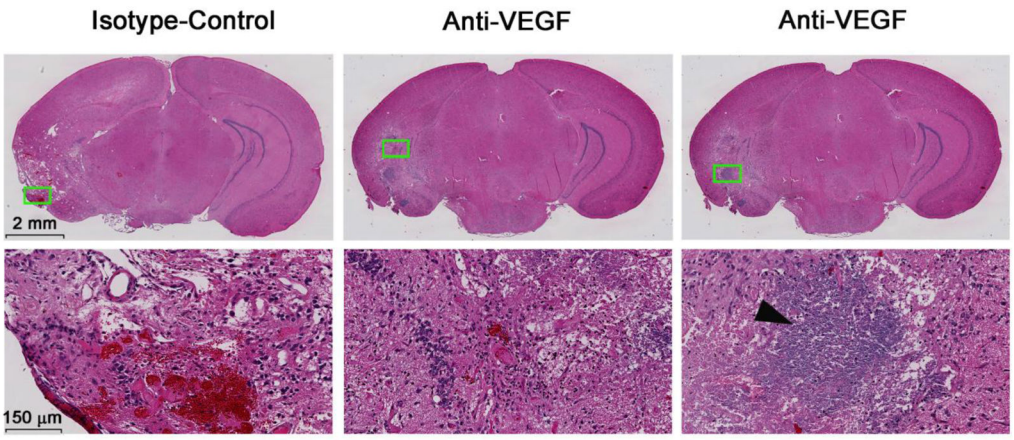

Fig. 3.

Representative 2× (*top*) and 20× (*bottom*) H&E-stained slides for one isotype-control antibody treated mouse (*left*) and one anti-VEGF antibody treated mouse, with two different magnified areas (*middle* and *right*, respectively) at week 12 PIR. Both groups show histologic features that are characteristic of radiation necrosis, including hemorrhage, telangiectasia, loss of tissue, and neuronal necrosis. Note the large area of focal calcification (*black arrowhead*) in the *bottom right* panel

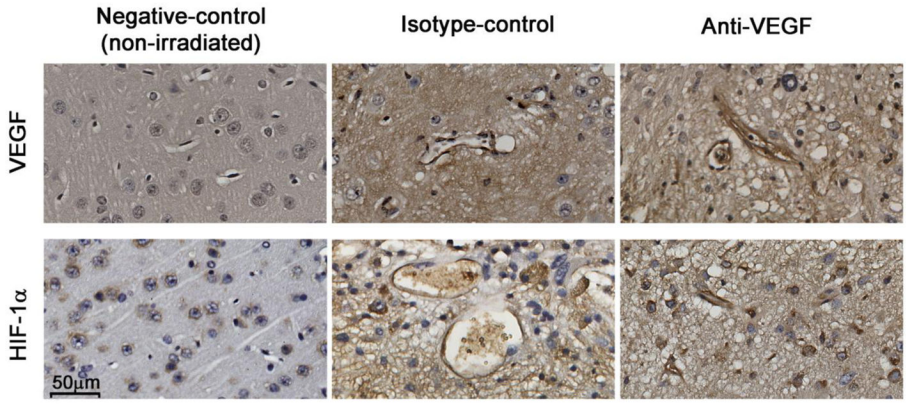

Fig. 4.

Representative 60× VEGF (*top*) and HIF-1α (*bottom*) staining for non-irradiated (*left*), isotype-control treated (*middle*) and anti-VEGF treated (*right*) mice. *Brown* indicates positive staining for both VEGF and HIF-1α. Note, in particular, the *dark brown* staining along the dilated vessel walls